We are thankful to the reviewer for his/her thoughtful and constructive comments that help improve the manuscript substantially. We have revised the manuscript accordingly. Listed below is our point-to-point response in blue to each comment that was offered by the reviewer.

Response to Reviewer #2

The manuscript " Mixing state and effective density of aerosol particles during the Beijing 2022 Olympic Winter Games " mainly investigates the impacts of emission controls on particle mixing state and density by deploying a single particle aerosol mass spectrometer in tandem with a differential mobility analyzer and an aerodynamic aerosol classifier during the Beijing 2022 Olympic Winter Games (OWG). In general, the paper is well written and presented in a logical way. It is of general interest for Atmospheric Chemistry and Physics related communities. I therefore recommend publication of this paper in Atmospheric Chemistry and Physics after some revisions. My comments are listed as follows:

Specific Comments:

Line 16: “showed” should be changes to “show”. Besides, I suggest the authors to use present tense in writing a scientific article. I recommend to use external proof reading before submission of the revised version.

Thanks to the reviewers for pointing this out, and we have revised it as suggested.

Lines 16-17: the meaning of “Total- EC”, “Total-OC” and “Total-ECOC” should be given here, also including other abbreviations (e.g., EC-NS, KEC-N, and ECOC-NS).

Thank the reviewer’s comments. We have added the meaning of the abbreviations in lines 17-21.

Line: 75-76: a detailed explanation for “DMA (model 3085A, TSI Inc.) and SPAMS (Hexin Analytical Instrument Co., Ltd.), AAC (Cambustion Ltd.)” should be given.

Thank the reviewer’s comments. We have added detailed explanations of the abbreviations of the three instruments in lines 77-79. In addition, we provide detailed descriptions of the three instruments in Section 1.1 of the supplementary.

Lines 88-89: “The detailed operations of AE33 and HR-ToF-AMS, and the data analysis are given in Xu et al. (in preparation).”, some descriptions are needed because the paper of Xu et al. is in preparation.

Thank the reviewer for pointing this out. The dried ambient particles were collected by HR-ToF-AMS and AE33 at flow rates of 1 and 5 L min^{-1} through stainless steel sampling lines (1/4 inch o. d.), respectively, and measured at time resolutions of 1 min in this study. Where the measurements of HR-ToF-AMS were performed under V-mode. The ionization efficiency (IE) was calibrated with ammonium nitrate particles (300 nm) and the elemental ratios of organic aerosols (OA) were

calculated with the "Improved-Ambient" method (Canagaratna et al., 2015; Jimenez et al., 2003; Jayne et al., 2000). The HR-ToF-AMS data were analyzed by using PIKA v 1.24, which showed that NO_3 (4.30 μg m^{-3}) and Org (3.80 μg m^{-3}) contributed 68.0 % of the mass concentration of NR-PM_1 (11.92 μg m^{-3}), followed by SO_4 (1.91 μg m^{-3}), NH_4 (1.69 μg m^{-3}), and Chl (0.22 μg m^{-3}). Thereafter, the sources of OA factors were resolved by using the positive matrix factorization (PMF) of high-resolution mass spectra of OA. Factors including fossil fuel combustion-related OA (FFBBOA), cooking OA (COA), and three SOA factors, i.e., two oxygenated OA (OOA1 and OOA2) and an aqueous-phase OOA were identified with mass concentrations of 0.31, 0.87, 0.83,1.18 and 0.56 μg m^{-3}, respectively. In addition, the mass concentration of equivalent black carbon (eBC) obtained by AE33 was calculated based on the dual-spot measurement (Drinovec et al., 2015; Rajesh and Ramachandran, 2018), with an average of 1.34 μg m^{-3} over the campaign. We have provided additional descriptions of the data analysis and operations of AE33 and HR-ToF-AMS in lines 89-97 as suggested. In addition, we have given the exact measurement values of AE33 and HR-ToF-AMS in the conclusion section when it is necessary to use them for specific demonstrations, e.g., lines 129 and 136, and Table 2 and S1.

Line 106: what are the sources of the two approaches of calculating the ρeff in this study? Besides, why do the authors use two approaches to calculate the ρeff?

Thank the reviewer's comments. As mentioned in the Response to Reviewer #1 above, we initially planned to connect DMA and AAC in tandem with SPAMS at different periods and select particles with D_m and D_a in the range of 150–300 nm and 200–700 nm, respectively, to finally obtain two complete datasets. However, only the SPAMS data with D_a = 300 nm were eventually credible in the AAC-SPAMS period, accounting for 13.3% of the total particles captured by SPAMS (322415 of 2416964). This was due to the unstable sheath flow of AAC when selecting particles in the size range of 400–700 nm, and only 1756 particles were captured at D_a = 200 nm due to the SPAMS detection limit. Considering that the data quality of the AAC-SPAMS period was unsatisfactory, we decided to combine the DMA-SPAMS and AAC-SPAMS data for the purpose of analyzing the data in order to ensure that the results of our study are representative. SPAMS, DMA and AAC can provide vacuum aerodynamic diameter (D_{va}), mobility diameters (D_m) and aerodynamic diameters (D_a) of particles, respectively. The relationship between these three diameters and the method for calculating the effective density (ρ_{eff}) of particles, which is obtainable when any two of these diameters are known, have been described in detail by Decarlo et al. (2004). For example, when the D_{va} and D_m of particles are available, the ρ_{eff} of particles can be calculated as follows:

$$\rho_{eff} = \frac{D_{va}}{D_m}\rho_0 \quad (12)$$

This equation can be adopted to calculate the ρ_{eff} of particles captured by the DMA-SPAMS tandem system, where ρ_0 is the standard density (1.0 g cm^{-3}). For the AAC-SPAMS tandem system, the ρ_{eff} is defined based on the ratio of the particle density (ρ_p) to the particle dynamic shape factor (χ_γ) as shown below:

$$\rho_{eff} = \frac{\rho_p}{\chi_\gamma} = \frac{D_{va}}{D_{ve}\rho_0} \quad (13)$$

The relationship between D_a, D_{va} and D_{ve} can be expressed by the following equation:

$$D_a = D_{ve}\sqrt{\frac{\rho_p C_c(D_{ve})}{\chi_t \rho_0 C_c(D_a)}} \quad (14)$$

where χ_t represents the aerosol dynamic shape factor in the transition regime. Considering the approximation between χ_t and χ_γ, the D_{ve} can be calculated by combining Eqs. (13) and (14) as follows:

$$C_c(D_a)\frac{D_a^2}{D_{va}} = D_{ve}C_C(D_{ve}) \quad (15)$$

$C_c(D)$ is the Cunningham slip correction factor, which can be calculated by the following equation:

$$Cc(D) = 1 + \frac{\lambda}{D}(A + B \cdot exp(\frac{C \cdot D}{\lambda})) \quad (16)$$

where λ represents the mean free path of the gas molecules. A, B and C are empirically determined constants specific to the analyzed system, where A is 2.33, B is 0.966 and C is -0.498. Substituting Eq. (16) into Eq. (15) obtains Eq. (17):

$$\frac{D_a^2}{D_{va}} + \frac{D_a \cdot \lambda}{D_{va}}\left(A + B \cdot exp\left(\frac{C \cdot D_a}{\lambda}\right)\right) = D_{ve} + \lambda\left(A + B \cdot exp\left(\frac{C \cdot D_{ve}}{\lambda}\right)\right) \quad (17)$$

The D_a and D_{va} are known in the AAC-SPAMS tandem system, which can be brought into Eq. (17) to obtain D_{ve}. Finally, the ρ_{eff} of particles captured by the AAC-SPAMS tandem system can be derived from Eq. (13). The accuracy of the above two methods of ρ_{eff} calculation has been verified in previous studies (Spencer et al., 2007; Su et al., 2021; Peng et al., 2021; Pagels et al., 2009; Katrib et al., 2005). We have provided additional explanations in Section 2.3.2 of the manuscript as suggested.

Lines 498-502: the meaning of wind direction (WD) values should be described; the colors in curves of eBC and NR-PM1 cannot be well distinguished; “hit rare” is “hit rate”? Why “both size and hit counts after 2.10 are divided by 4”? Additionally, all the meaning of symbols (e.g., green cross in Fig. 1a) and lines (e.g., blue and green lines with arrows in Fig. 1a) occurred in figures should be described.

Thank the reviewer’s comments. Wind direction is measured in degrees clockwise from due north (e.g. 0 degrees for a northerly wind and 270 degrees for a westerly wind) and has been explained on line 542 as suggested. In addition, the NR-PM_1 curve has been changed to red in the figure to distinguish it better. Line 543 was originally intended to express “hit rate”, and we thank the reviewer for pointing out this spelling error. Only particles with D_a of 300 nm were selected for data analysis in the AAC-SPAMS period, which is indicated by a blue arrow at the top of Fig. 2. While particles with D_m of 200, 250, 300, and 150 nm were sequentially selected in the DMA-SPAMS period, indicated by four green arrows at the top of Fig. 2. The yellow and gray shading in the figure

represent the snowfall period and the Olympic Winter Games period, respectively. The meaning of the above elements in the figure has been further explained in lines 546-547.

As described in Section 2.1 of the manuscript, SPAMS was connected in tandem with DMA (21 January to 10 February) and AAC (10 February to 1 March) at different periods. Since the measurements of the DMA are performed by a force balance between the electrical force of a constant electric field on the net charges on the particle and the drag force experienced by the particle. Whereas the AAC selects particles based on aerodynamic sizes according to particle relaxation time without needing charging for electrostatic. In other words, DMA has more stringent conditions for particle selection than AAC, and more particles will be captured by SPAMS through AAC under the same circumstances. This is consistent with the results of this study, with average size and hit counts per minute of 49 and 16 when SPAMS was in tandem with DMA, compared to 396 and 84 when SPAMS was in tandem with AAC. The SPAMS hit rate was slightly different between the two periods (32.65% vs. 21.21%), which is attributed to the decrease in the hit rate due to the high pass rate of the AAC. However, if the time series of size and hit counts were plotted directly as shown in Fig. R4, the trend in the DMA-SPAMS period would be quite insignificant because too few particles were captured per minute compared to the AAC-SPAMS period. Therefore, in order to show the temporal trends of size and hit counts during the DMA-SPAMS period more visually, we reduced the data after 10 February to one-fourth of the original values. Additional explanations have been provided in lines 543-544 as suggested.

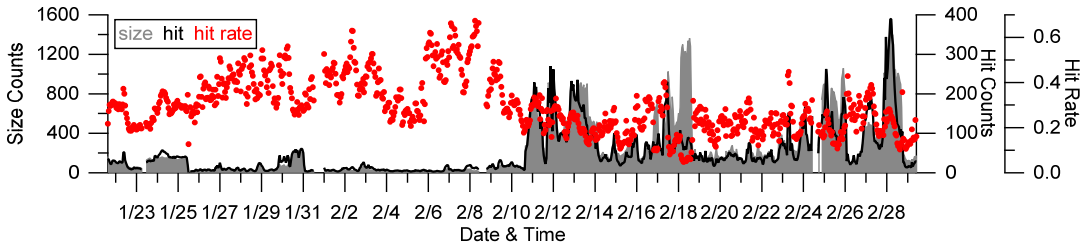

Figure R4: Time series of the number of sized particles, hit particles as well as the averaged hit rate of SPAMS per minute.

Line 158: “diurnal cycle” could be more reasonable than “diurnal trend”.

Changed as suggested.

Line 254-255: Why did the emission controls during OWG lead to the increases in aged and regional particles? A reason analysis is expected in discussions. Thus, corresponding to the data analysis results, an analysis of mechanism behind the phenomenon is needed.

Thank the reviewer’s comments. To improve air quality during the OWG period, the government took radical actions to reduce emissions from major sources (including industry, coal combustion, and transportation, among others), which resulted in a significant decrease in the number concentrations of particles captured during the OWG (Table S2). The number concentration of

Total-EC particles decreased by 61.80% during the OWG, which was much higher than 20.28% for Total-ECOC and 28.74% for Total-OC. Although emission control led to the overall decrease in the number concentration of particles during the OWG period, the role of aging and regional particles became more prominent. Especially for ECOC-NS particles, the particle counts of daily captures increased by 17.34% during the OWG period compared to the nOWG period. In addition, bivariate polar plots for most classes of particles show that the high number concentrations were concentrated at the sampling site during the nOWG period, while the source locations were skewed to the southeast or southwest during the OWG period. The $PA_{sulfate}/PA_{nitrate}$ of primary particles (e.g., KOC-N, HM, Biomass-K, etc.), which were determined by combining mass spectra, daily trends, and correlations with OA factors, were higher during the OWG period than during the nOWG period. This indicates that emission controls significantly reduce local primary emitted particles, resulting in significant aging and regional characteristics despite the small number concentrations of particles captured. We added Table S2 to the supplementary with the purpose of comparing the daily capture of different classes of particles during the OWG and nOWG periods. Additional explanations are also provided in lines 139-143.

Table S3: A summary of particle types and number of particles captured per day for the OWG and nOWG periods.

Classification of particles		OWG	nOWG	OWG (per day)	nOWG (per day)
Total-EC	pure-EC	1155	2162	68	94
	EC-NS	8845	39761	520	1729
	KEC-N	4947	21303	291	926
	KNaEC-N	7039	14037	414	610
Total-ECOC	ECOC-NS	50382	58108	2964	2526
	KECOC-CN	3602	4891	212	213
	KECOC-NS	60631	109959	3567	4781
	KNaECOC-NS	13725	22096	807	961
	KAECOC-NS	662	23314	39	1014
Total-OC	KOC-N	13078	25298	769	1100
	KOC-NS	12242	18998	720	826
	K-Amine-NS	1219	6446	72	280
Total-IA	K-N	11561	24385	680	1060
	KNa-N	6215	9693	366	421
Biomass-K		41627	54526	2449	2371
HOM		16610	24388	977	1060
Metals	rich-Fe	1474	14088	87	613
	other	3542	7245	208	315

A discussion on the uncertainties of data quality and analysis should be included in the "conclusions" section.

Thanks to the reviewer for pointing this out. Although the real-time on-line measurement of the size and chemical composition of individual particles can be achieved by SPAMS, the ionizing laser has different sensitivities for the detection of different chemical compositions. For example, the ionizing laser is sensitive to alkaline metals (e.g., potassium and sodium) and elemental carbon particles with strong light absorption, leading to differences in the quantification of different chemical compositions. It is necessary to pay more attention to the evaluation of quantitative analysis of

SPAMS in the future. We have added discussion of instrumental uncertainty in lines 285-287 as suggested.

References

Canagaratna, M. R., Jimenez, J. L., Kroll, J. H., Chen, Q., Kessler, S. H., Massoli, P., Hildebrandt Ruiz, L., Fortner, E., Williams, L. R., Wilson, K. R., Surratt, J. D., Donahue, N. M., Jayne, J. T., and Worsnop, D. R.: Elemental ratio measurements of organic compounds using aerosol mass spectrometry: characterization, improved calibration, and implications, Atmos. Chem. Phys., 15, 253–272, doi:10.5194/acpd-14-19791-2014, 2015.

Drinovec, L., Močnik, G., Zotter, P., Prévôt, A. S. H., Ruckstuhl, C., Coz, E., Rupakheti, M., Sciare, J., Müller, T., Wiedensohler, A., and Hansen, A. D. A.: The "dual-spot" Aethalometer: an improved measurement of aerosol black carbon with real-time loading compensation, Atmos. Meas. Tech., 8, 1965-1979, doi:10.5194/amt-8-1965-2015, 2015.

Jimenez, J. L., Jayne, J. T., Shi, Q., Kolb, C. E., Worsnop, D. R., Yourshaw, I., Seinfeld, J. H., Flagan, R. C., Zhang, X., Smith, K. A., Morris, J. W., and Davidovits, P.: Ambient aerosol sampling using the Aerodyne Aerosol Mass Spectrometer, J. Geophys. Res. , 108, 8425, doi:10.1029/2001jd001213, 2003.

Rajesh, T. A. and Ramachandran, S.: Black carbon aerosol mass concentration, absorption and single scattering albedo from single and dual spot aethalometers: Radiative implications, J. Aerosol Sci., 119, 77-90, doi:10.1016/j.jaerosci.2018.02.001, 2018.